

Article

Photocatalytic Properties of g-C₃N₄-Supported on the SrAl₂O₄:Eu,Dy/SiO₂

Shielah Mavengere  and Jung-Sik Kim *

Department of Materials Science and Engineering, University of Seoul, Seoul 02504, Korea; lashiema@gmail.com

* Correspondence: jskim@uos.ac.kr; Tel.: +82-2-6490-2409

Received: 28 August 2020; Accepted: 22 September 2020; Published: 24 September 2020



Abstract: Graphitic carbon nitride (g-C₃N₄) was supported on SrAl₂O₄:Eu,Dy-SiO₂ by a colloidal-sol coating method to improve its light absorption property. Transmission electron microscopy (TEM) revealed that the nanoparticles of g-C₃N₄ were coated on sub-micron phosphor particles and nanoscale surface roughness was imparted by the SiO₂-binder. Photoluminescence (PL) spectrum of the g-C₃N₄ supported on SrAl₂O₄:Eu,Dy exhibited a broadband emission from 400 to 650 nm. Increasing silica-binder in the g-C₃N₄/SrAl₂O₄:Eu,Dy composites suppressed the PL emission peak at 525 nm for SrAl₂O₄:Eu,Dy. Photocatalytic degradation activity was evaluated with 5 ppm methylene blue (MB) solutions under germicidal ultraviolet (UV) and visible (Vis) solar light illuminations. The UV/Vis photocatalytic efficiency was improved by supporting g-C₃N₄ on the SrAl₂O₄:Eu,Dy phosphor and with the addition of SiO₂ as a binder. In addition, low silica addition effectively improved the adhesiveness of the g-C₃N₄ coating on the SrAl₂O₄:Eu,Dy surface. Recyclability tests of photocatalysis for the SrAl₂O₄:Eu,Dy-0.01M SiO₂/50wt% g-C₃N₄ composites exhibited a remarkable stability by maintaining the degradation efficiencies above 90% in four cycles. Therefore, the composite of g-C₃N₄-supported SrAl₂O₄:Eu,Dy-SiO₂ is a prospective photocatalyst activating under UV/Vis light irradiation for the elimination of environmental pollutants.

Keywords: g-C₃N₄; SrAl₂O₄:Eu,Dy phosphor; colloidal-sol coating; SiO₂; UV-visible light photocatalysis

1. Introduction

Nano-based materials technologies offer promising methods for harnessing solar energy to tackle air and water pollution problems. In the past decades, the trending researches were based on employing TiO₂ semiconductors in photocatalysis applications [1,2]. Apart from this UV-activated material, the graphitic carbon nitride (g-C₃N₄) organic semiconductor is reportedly a versatile material for efficiently utilizing a broader visible light solar spectrum. A band gap of 2.7 eV insinuates the g-C₃N₄ non-metallic compound to absorb visible light of ~460 nm and facilitate photocatalytic reactions [3]. Additionally, significant research attention has been focused on g-C₃N₄ attributable to its easy, low-cost fabrication from carbon-nitrogen (C-N) rich precursors, such as urea [4], dicyandiamide [5], and melamine [6]. However, the bulk g-C₃N₄ metal-free photocatalyst provides small specific surface areas to volume ratio, slow reaction kinetics and fast charge recombination [7,8].

In an effort to reduce the bulkiness of g-C₃N₄, researchers have conducted experiments through mechanical ball milling, chemical, ultrasonic-assisted, and thermal exfoliation methods [9–12]. Coupling the exfoliated g-C₃N₄ with other compounds remarkably forms hybrid materials with unique heterojunctions. For instance, mesoporous g-C₃N₄/TiO₂ [13], g-C₃N₄/N-TiO₂ [14], amorphous SiO₂ with g-C₃N₄ [15], YVO₄/g-C₃N₄ [16], g-C₃N₄/SiO₂-SnO₂ [17], and MoS₂/Al₂O₃/g-C₃N₄ [18] hybrid/ternary composites showed improvements in photoactivity. It is emphasized that heterojunctions existing at the interfacial periphery of g-C₃N₄ and the coupled compounds play an important role in light

sensitization and providing a pathway for electron-hole separation [19–22]. Therefore, hybrid/ternary composites with g-C₃N₄ have great potential in solving pollution related problems [23–25].

One compound which has received tremendous attention in phosphorescent display materials and as a thermally stable catalyst support is a rare-earth doped phosphor [26,27]. Precisely, strontium aluminate phosphor materials such as Sr₄Al₁₄O₂₅:Eu,Dy [26,28,29] and SrAl₂O₄:Eu,Dy produce an aesthetic visible light (blue or green, respectively) after UV-light excitation [30]. Recent studies revealed that solution combustion method is a robust method for synthesizing strontium aluminate phosphor with nanoparticle size distribution [31]. Although strontium aluminate phosphors are referred to as a physicochemical stable support for improved catalytic efficiencies [29,32], the effects of supporting g-C₃N₄ on SrAl₂O₄:Eu,Dy have not been extensively studied. Additionally, g-C₃N₄ catalyst is allegedly a futuristic material for solving pollution related problems at a large scale with minimal cost-constraint [33–35]. Therefore, it is necessary to further investigate on the effect of coupling the strontium aluminate phosphor with g-C₃N₄. Another notable advantage of coupling g-C₃N₄ nanoparticles with a 20–100 μm phosphor support is the possible improvement in density of nanocomposites [30]. This way, the recyclability of nanocomposites by sedimentation significantly reduces secondary polluting problems related to nanoparticles application [36,37]. In consequence, nanocomposites photocatalyst applications are broadened in solving organic pollutants in aquatic systems.

SrAl₂O₄:Eu,Dy phosphors have unique light scattering property which is beneficial for energy harvesting [38]. Moreover, SrAl₂O₄:Eu,Dy typically possess a long after-glow which has been reported to even sustain photocatalytic activity in visible light and in dark state [39,40]. Since high temperature sintering of phosphor reduces porosity, a buffer binding layer such as SiO₂ is necessary to improve adhesion of the g-C₃N₄ catalyst. Additionally, SiO₂ coatings on SrAl₂O₄:Eu,Dy prevents the degradation of O-Sr-O bonds in an aqueous environment [41]. SiO₂ is popularly known for high surface areas and has been coupled with other compounds at weight percent ratios (wt.%) showing good photocatalytic performance [15]. However, adding SiO₂ in molar ratio to SrAl₂O₄:Eu,Dy/g-C₃N₄ have not been studied.

In this study, the g-C₃N₄ was supported on SrAl₂O₄:Eu,Dy phosphor with aid of SiO₂ as a binding agent. The photocatalytic performance was evaluated with respect to amount of g-C₃N₄ on SrAl₂O₄:Eu,Dy phosphor with or without silica binder under ultraviolet (UV) and visible light activation. Photocatalyst reusability studies were also conducted to evaluate the practicality of repeatedly using the SrAl₂O₄:Eu,Dy-SiO₂/g-C₃N₄ composite in mitigating pollutants.

2. Materials and Methods

SrAl₂O₄:Eu,Dy long-lasting phosphor for supporting graphitic carbon nitride (g-C₃N₄) catalyst was synthesized by solution combustion method. Strontium aluminate-sol was prepared by mixing Sr(NO₃)₂ (97.0%, Junsei Chemical Co., Ltd., Tokyo, Japan) and Al(NO₃)₂•9H₂O at 0.95/1 molar ratio (98.0% Yakuri Pure Chemicals Co., Ltd., Kyoto, Japan) in 20 mL distilled water (D.I = H₂O) at 60 °C for 30 min. At the same time, Eu/Dy rare earth-sol was prepared in a separate 50-mL beaker from a 0.02/0.03 molar ratio of Eu₂O₃/Dy₂O₃ (99.99%, Sigma-Aldrich, St. Louis, MO, USA), respectively, and nitric acid (70%, Daejung Chemicals & Metals Co., Ltd., Siheung-si, Gyeonggi-do, Korea). After a 10-min stirring procedure at 60 °C, 4 wt.% B₂O₃ (Sigma-Aldrich, St. Louis, MO, USA) and 2 wt.% urea (99.0%, Samchun Pure Chemicals Co., Ltd., Pyeongtaek, Gyeonggi-do, Korea) were promptly added with continuous mixing for 20 min. The Sr-Al-nitrate sol and Eu/Dy rare earth-sol were further mixed in a beaker at 120 °C to form a thick multi-element solution. A 5-min electric muffle furnace (SK1700-B30, Thermotechno Co., Siheung-si, Gyeonggi-do, Korea) combustion process was performed at 600 °C in a closed crucible to obtain yellowish-fluffy SrAl₂O₄:Eu,Dy powders. Additionally, obtained powders were ground with pestle-mortar and finally sintered in an electric tube furnace (AH Jeon Industrial Co., Namyangju-si, Gyeonggi-do, Korea) with N₂-H₂ (95% N₂, 5% H₂, Union gas, Yongin-si, Gyeonggi-do, Korea) reducing gas atmosphere at 1100 °C for 1 h. Dried SrAl₂O₄:Eu,Dy powders

were further pulverized by high-energy grinding in a Planetary Mono Mill (Fritsch Pulverisette-6, Idar-Oberstein, Germany) for 1 h at 450 rpm to reduce agglomeration prior to catalyst coating.

The SiO₂-binding-sol was prepared from a tetraethyl orthosilicate (TEOS) precursor (98%, Sigma-Aldrich, St. Louis, MO, USA). In this process, 16 mL ethanol (Duksan Pure Chemicals Co., Ansan-si, Kyunggi-do, Korea), 4 mL D.I water, and 0.8 mL NH₄OH (30%, Duksan Pure Chemicals Co., Ansan-si, Kyunggi-do, Korea) were magnetically stirred in a 50-mL beaker at 30 °C. After 10-min stirring, 0.16 mL TEOS was added drop-wise to the alkaline solution. Then, SiO₂-sol was thoroughly mixed with ultra-sonic agitation (Powersonic 510, 10L, DH-D250H, Daihan Scientific, Wonju-si, Gangwon-do, Korea). Batches of 0.25 g SrAl₂O₄:Eu,Dy phosphor were coated with varying silica-sol (0.005, 0.01, 0.02, 0.1, and 0.2) molar concentration by dip coating for 10 min with ultrasonic-treatment. This was followed by centrifuging at 5000 rpm for 5 min to remove excess ethanol solution. The obtained SrAl₂O₄:Eu,Dy.SiO₂ samples were dried at 100 °C for 6 h and calcined at 400 °C for 2 h.

For the synthesis of carbon nitride (g-C₃N₄) catalyst, 5 g of melamine (99.0%, Duksan Pure Chemicals Co., Ansan-si, Kyunggi-do, Korea) was thermally decomposed in a muffle furnace at 550 °C for 2 h. The yellow bulky g-C₃N₄ product was pulverized for 1 h in a pulveriser at 450 rpm (Fritsch, DE/pulverisette 23 mini mill) to increase surface area. The g-C₃N₄ was exfoliated by ultrasonic treatment for 30-min in glass vials with 10 mL ethanol. The g-C₃N₄ impregnation-sol was prepared for coating comparison batches with varying SiO₂-binder coating on SrAl₂O₄:Eu,Dy phosphor. The g-C₃N₄ impregnation on SrAl₂O₄:Eu,Dy proceeded as a wet coating step, where 2 g of phosphor was dispersed with ultrasonic treatment in 10 mL g-C₃N₄ sol were coated with the colloidal g-C₃N₄ solution and calcined at 450 °C for 2 h.

SrAl₂O₄:Eu,Dy-SiO₂/g-C₃N₄ composites were analyzed for crystallinity and morphology by X-ray diffraction (XRD) with Cu K α radiation (Bruker AXS8 Advanced, D8 Discover, Bruker AXS GmbH, Karlsruhe, Germany) and Scanning Electron Microscopy (SEM, Hitachi S-4300, Hitachi Ltd., Tokyo, Japan), respectively. High resolution textural properties and elemental mappings were evaluated by transmission electron microscopy (TEM) model JEM-2010/JEOL JP with inbuilt Elemental Dispersive Spectroscopy (EDS). UV-Vis diffuse reflectance absorption characteristics of solid photocatalyst samples were analyzed by UV-VIS-NIR Spectrophotometer (UV-3150 Shimadzu, Kyoto, Japan). The photoluminescence (PL) spectra were obtained from a fluorescence spectrophotometer (Hitachi F-4500, Tokyo, Japan) under 350 nm Xe excitation wavelengths at 2.5 nm emission slit width. The specific surface area and porosity of the nano crystalline g-C₃N₄, SrAl₂O₄:Eu,Dy/g-C₃N₄ and SrAl₂O₄:Eu,Dy-0.01M SiO₂/g-C₃N₄ were determined by Brunauer–Emmett–Teller (BET) and Barrett–Joyner–Halenda (BJH) methods on a Micropore Physisorption/Chemisorption Analyzer (AUTOSORB-IQ-MP).

UV-light photocatalytic activity was evaluated on 2 mg/mL catalyst to methylene blue (MB) solution. The 5 ppm methylene blue dye, (MB, 95%, Duksan Pure Chemical Co., Ansan-si, Kyunggi-do, Korea) organic pollutant was placed in a beaker with photocatalyst composite and stirred in the dark to attain adsorption equilibrium. The photo-reaction was initiated under 8 W UV germicidal lamp (Sankyo Denki Co, Kanagawa, Japan) illuminations and at 1-h interval 2 mL samples were pipetted for absorption measurements. Figure S1 shows spectra for UV light. The photocatalyst reaction mixture was exposed to 254 nm UV illuminations until MB solution was decolorized. UV-VIS-NIR spectrophotometer (UV-3150 Shimadzu, Kyoto, Japan) was used to measure the MB absorption variation for the photodegradation cycles for different photocatalyst samples.

Visible light photoactivity was evaluated on reaction mixtures prepared from 1 mg/mL of catalyst/MB solution (5 ppm). Then, the photoreaction mixture was placed in a stainless steel Luzchem Solar Simulator (SOLSIM2, Ottawa, Ontario, Canada) with a 300 W Xe lamp. Figure S2 shows the Xe lamp spectra (Solsim 395). The UV-light photons were cut-off with a 410 nm filter (UV L41 (W) 82 mm, Kenko Zeta, Tokina Co., Tokyo, Japan) and the light intensity was fixed at 6000 lux. The solar simulator shutter was closed and 2 mL sample was pipetted at 15-min intervals until the MB solution decolorized. The UV-Vis measurements were analyzed as explained in UV-light photocatalyst tests.

Photocatalytic reusability tests were performed to evaluate the extent of catalyst photostability and suitability for long-term use in pollutants mitigation. The recycling tests were investigated on 50 wt.% g-C₃N₄ supported on SrAl₂O₄:Eu,Dy-0.01M SiO₂ samples in 5 ppm MB solution at 2 mg/mL of catalyst/MB loading ratio. Procedures explained in UV-photocatalysis were followed to photo activate and collect reaction mixture samples. However, after 240 min of photoactivity, the catalyst was centrifuge collected, washed in ethanoic solution, rinsed with distilled water and dried in an electric oven. At 2 mg/mL catalyst/MB dye ratio, the catalyst was reused again in the photo-reaction mixture to degrade MB-dye solutions for 3-cycles (240-min per cycle) with after cycle wash-centrifuge steps. Finally, the 2-mL aliquot samples for four cycles were measured by a UV-VIS-NIR spectrophotometer (UV-3150, Shimadzu, Kyoto, Japan) for methylene blue absorbance variation.

3. Results

Figure 1 exhibits the XRD patterns for bulk g-C₃N₄ and nano crystalline g-C₃N₄ supported on the SrAl₂O₄:Eu,Dy phosphor. Bulk graphitic carbon nitride has crystallinity as shown by two peaks indexed (100) at 13.3° and (002) at 27.5° in reference to JCPDS 87-1526. SrAl₂O₄:Eu,Dy is crystalline with characteristic peaks labelled in reference to JCPDS 34-0379. The SrAl₂O₄:Eu,Dy phosphor peaks at (211), (031) and (222) weakened with additional g-C₃N₄ and both g-C₃N₄-SiO₂ coating. This confirms the amorphous nature of SiO₂ as well as the overall decrease of phosphor host matrix compared to pure phosphor sample. The nano crystalline g-C₃N₄/SrAl₂O₄:Eu,Dy with or without silica only contained phosphor peaks. The absence of nano crystalline g-C₃N₄ confirms the bulk structure changed to amorphous during the pulverization milling and ultrasonic exfoliation to reduce agglomeration. Additionally, the nano crystalline g-C₃N₄ was beyond the XRD detection limit as supported on sub-micron phosphor matrix and also with the amorphous nature of silica. The disappearance of g-C₃N₄ peaks in composite materials has been observed in other researches, with an increase in the amount of the crystalline [16,42] or amorphous SiO₂ [43].

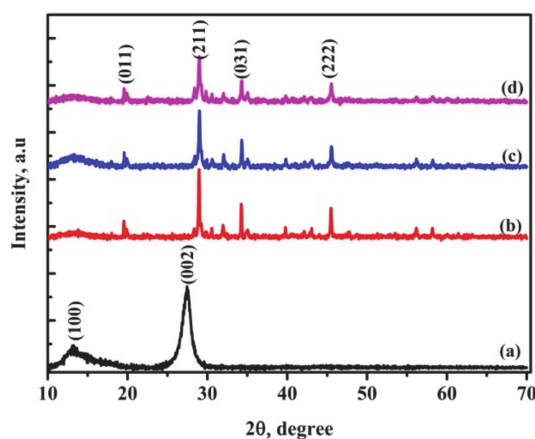


Figure 1. XRD patterns for (a) bulk g-C₃N₄ (b) SrAl₂O₄:Eu,Dy (c) SrAl₂O₄:Eu,Dy/50 wt.% g-C₃N₄ and (d) 50 wt.% g-C₃N₄ supported on SrAl₂O₄:Eu,Dy-0.01M SiO₂.

Figure 2 shows SEM images of (a) bulk g-C₃N₄, (b) SrAl₂O₄:Eu,Dy, and (c) SrAl₂O₄:Eu,Dy- 15 wt.% g-C₃N₄. The bulk g-C₃N₄ in Figure 2a are aggregates of several micrometers while SrAl₂O₄:Eu,Dy phosphor powders in Figure 2b show agglomerated particles of around few micrometers due to 1100 °C sintering temperature. However, Figure 2c shows the composite of g-C₃N₄/SrAl₂O₄:Eu,Dy in which the nano crystalline g-C₃N₄ particles are coated well partly on the SrAl₂O₄:Eu,Dy.

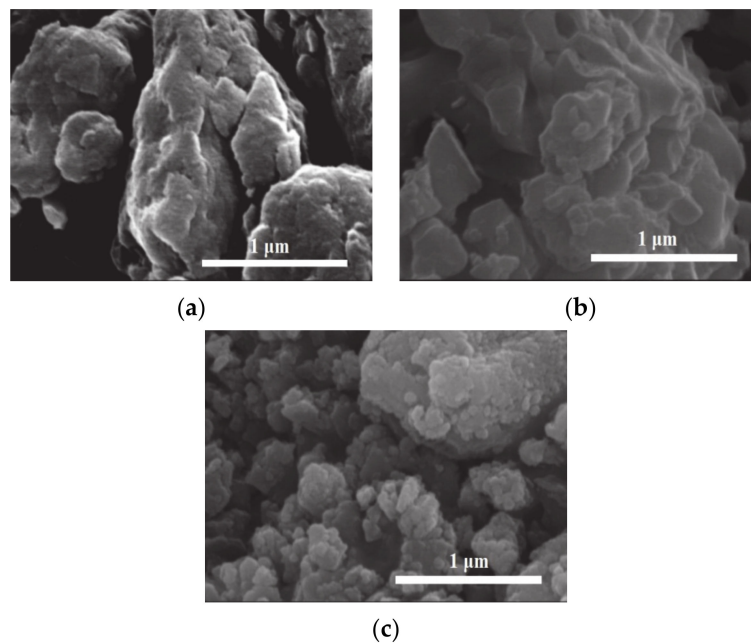


Figure 2. SEM images (a) g-C₃N₄ (b) SrAl₂O₄:Eu,Dy and (c) SrAl₂O₄:Eu,Dy/15 wt.% g-C₃N₄.

Figure 3 shows TEM, EDS spectra and elemental composition of the g-C₃N₄ supported on phosphor. Figure 3a shows TEM image of phosphor particles encapsulated with g-C₃N₄, where the black-contrast micro-particle is phosphor whilst the grey voluminous encapsulate with light-contrast is g-C₃N₄. The EDS spectra in Figure 3b confirm that all chemical elements are present in respective element compositions in Table 1. However, the composite of g-C₃N₄-coated SrAl₂O₄:Eu,Dy/SiO₂ in Figure 3c has nanoscale surface roughness as compared to g-C₃N₄-supported on SrAl₂O₄:Eu,Dy without silica. This surface roughness is accredited to SiO₂-binding which improves the stability of SrAl₂O₄:Eu,Dy/g-C₃N₄ adhesion. Surface-surface interaction of compounds is further indication of improvement of physiochemical properties which is major advantage of coupling materials. Figure 3d and Table 2 confirm that all chemical elements in SrAl₂O₄:Eu,Dy-SiO₂/g-C₃N₄ were present.

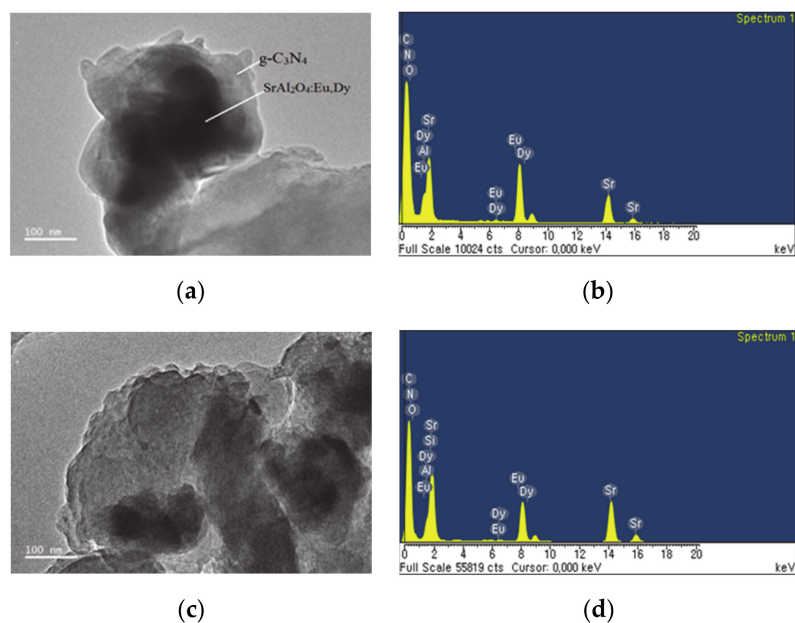


Figure 3. TEM images (a,c) and EDS spectra (b,d) where (a,b) is SrAl₂O₄:Eu,Dy/50 wt.% g-C₃N₄ and (c,d) is 50 wt.% g-C₃N₄ supported on SrAl₂O₄:Eu,Dy-0.01M SiO₂.

Table 1. Elemental analysis for SrAl₂O₄:Eu,Dy/50 wt.% g-C₃N₄.

Element	Weight%	Atomic%
C	43.35	58.24
N	23.54	27.11
O	8.37	8.45
Al	4.19	2.5
Sr	19.44	3.58
Eu	0.88	0.09
Dy	0.23	0.02
Totals	100	-

Table 2. Elemental analysis for 50 wt.% g-C₃N₄ supported on SrAl₂O₄:Eu,Dy-0.01M SiO₂.

Element	Weight%	Atomic%
C	55.67	71.29
N	21.34	23.43
O	0.94	0.91
Al	1.08	0.62
Si	0.41	0.23
Sr	19.51	3.42
Eu	0.97	0.1
Dy	0.07	0.01
Totals	100	-

Figure 4 shows the nitrogen adsorption-desorption isotherms for (a) nano crystalline g-C₃N₄, (b) SrAl₂O₄:Eu,Dy and (c) 50 wt.% g-C₃N₄-supported on SrAl₂O₄:Eu,Dy-0.01M SiO₂. Figure 4 adsorption-desorption graphs are similar to type (III) hysteresis loop. As shown in the figures, the g-C₃N₄, SrAl₂O₄:Eu,Dy and SrAl₂O₄:Eu,Dy-0.01M SiO₂/50 wt.% g-C₃N₄ samples are mesoporous since average pore diameter is in a range of 2 to 50 nm. The invariant pore diameter further confirms that the phosphor is a pore-free crystalline supporter and a silica binder insignificantly affects the composite porosity. Table 3 exhibits the BET specific surface area, BJH pore volume, and pore diameter for g-C₃N₄, SrAl₂O₄:Eu,Dy and 50 wt.% g-C₃N₄-supported on SrAl₂O₄:Eu,Dy-0.01M SiO₂. Accordingly, BET specific surface areas for nano crystalline g-C₃N₄, SrAl₂O₄:Eu,Dy and SrAl₂O₄:Eu,Dy-0.01M SiO₂/50 wt.% g-C₃N₄ were 14.9 m²/g, 13.2 m²/g and 11.7 m²/g, respectively. The specific surface area and pore volume decreased on samples coupled with crystalline phosphor and silica binder. This is justified to the volumetric bulkiness of phosphor-support and calcination procedure which causes particle coalescence as confirmed SEM morphology in Figure 2b. The BJH pore diameters for g-C₃N₄, SrAl₂O₄:Eu,Dy, and SrAl₂O₄:Eu,Dy-0.01M SiO₂/50 wt.% g-C₃N₄ were 3.81 nm, 3.80 nm, and 3.82 nm, respectively.

Table 3. BET specific surface area, BJH pore volume and pore diameter for the catalysts.

Sample	Surface Area m ² /g	Pore Volume cm ³ /g	Pore Diameter nm
a. g-C ₃ N ₄	14.9	0.14	3.81
b. SrAl ₂ O ₄ :Eu,Dy	13.2	0.08	3.80
c. SrAl ₂ O ₄ :Eu,Dy-0.01M SiO ₂ /50 wt% g-C ₃ N ₄	11.7	0.09	3.82

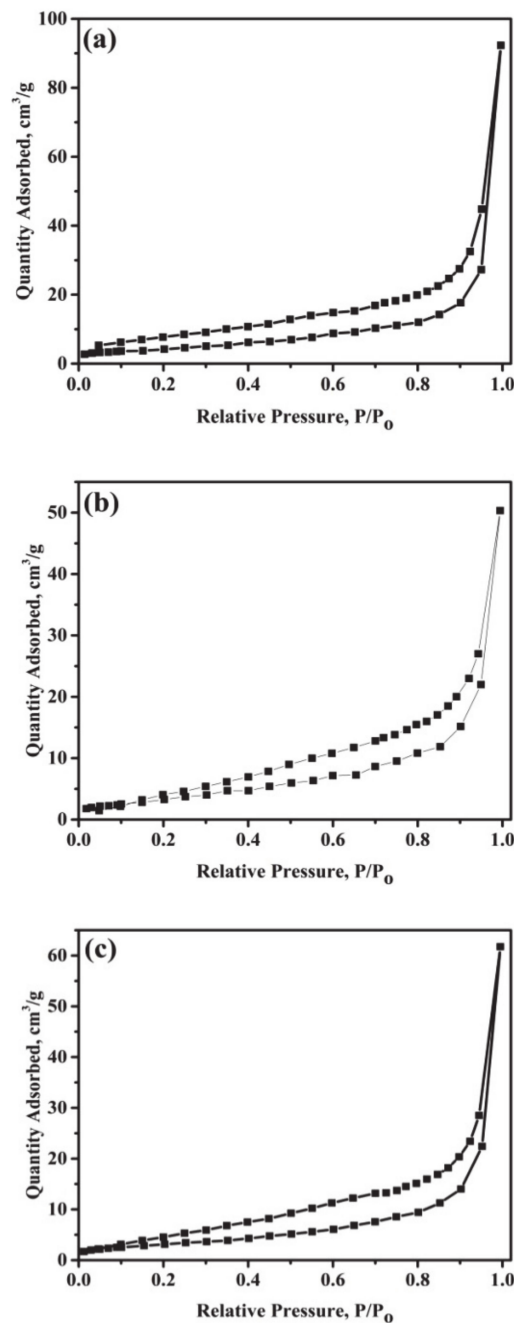


Figure 4. Nitrogen adsorption-desorption isotherms for (a) $g\text{-C}_3\text{N}_4$ (b) $\text{SrAl}_2\text{O}_4:\text{Eu,Dy}$ and (c) 50 wt.% $g\text{-C}_3\text{N}_4$ supported on $\text{SrAl}_2\text{O}_4:\text{Eu,Dy}-0.01\text{M SiO}_2$.

Figure 5 shows the diffuse reflectance absorption spectra for $g\text{-C}_3\text{N}_4$ in comparison with various amounts of $g\text{-C}_3\text{N}_4$ supported on $\text{SrAl}_2\text{O}_4:\text{Eu,Dy}$. The bulk $g\text{-C}_3\text{N}_4$ sample exhibits a strong UV optical absorption edge at 460 nm corresponding to the band gap of 2.7 eV as referenced by other researchers [24,44]. $\text{SrAl}_2\text{O}_4:\text{Eu,Dy}$ phosphor has strong absorption peak in the UV-Vis region. However, with increasing amount of $g\text{-C}_3\text{N}_4$ on phosphor surface, the peak absorption intensity is enhanced. Moreover, a shift towards the visible light region increased with increase in $g\text{-C}_3\text{N}_4$ on phosphor. The $\text{SrAl}_2\text{O}_4:\text{Eu,Dy}/50\text{ wt.}\% g\text{-C}_3\text{N}_4$ exhibits the largest shift as compared to other samples. This is a typical result of coupling compound materials, since each compound incorporates individual characteristic to the hybrid system.

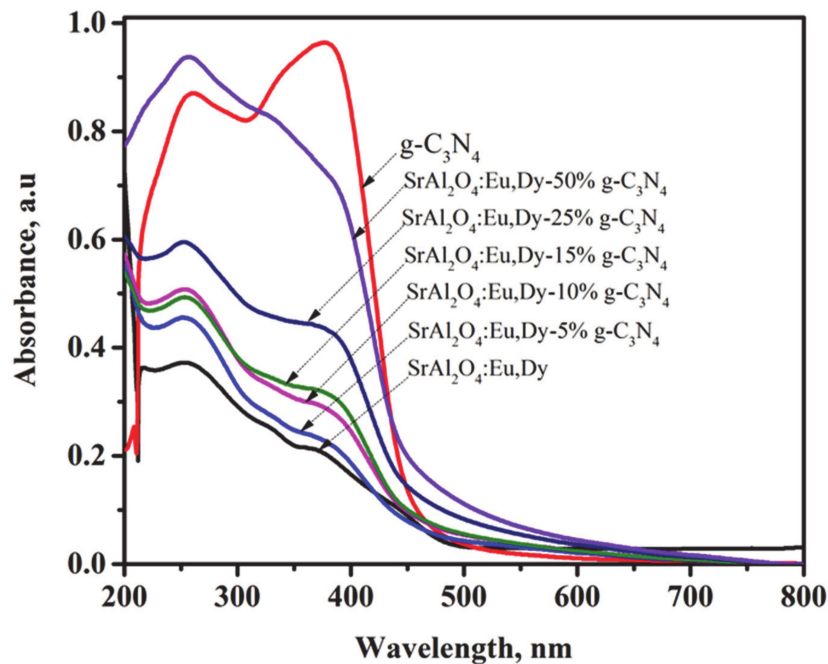


Figure 5. Diffuse reflectance absorption spectra for $g\text{-C}_3\text{N}_4$ and $\text{SrAl}_2\text{O}_4:\text{Eu,Dy}$ hybrid composites.

Figure 6a shows photoluminescence emission spectra for $g\text{-C}_3\text{N}_4$ supported on $\text{SrAl}_2\text{O}_4:\text{Eu,Dy}$ phosphor. The $g\text{-C}_3\text{N}_4$ and $\text{SrAl}_2\text{O}_4:\text{Eu,Dy}$ emission peak is maximum at 455 nm and 525 nm, respectively. Supporting $g\text{-C}_3\text{N}_4$ on $\text{SrAl}_2\text{O}_4:\text{Eu,Dy}$ suppresses the 525 nm-peak owing to energy transfers as observed in $\text{CuO}/\text{phosphor}$ [45]; or dissipation as well as emission light blockage effect similar to phosphor/ TiO_2 [46]. This also further confirms the successful encapsulation of phosphor with $g\text{-C}_3\text{N}_4$. As the amount of $g\text{-C}_3\text{N}_4$ on $\text{SrAl}_2\text{O}_4:\text{Eu,Dy}$ increases, the overall phosphor amount in the $\text{SrAl}_2\text{O}_4:\text{Eu,Dy}/g\text{-C}_3\text{N}_4$ composite decreases. As a consequence, the overall light absorption capacity by $\text{SrAl}_2\text{O}_4:\text{Eu,Dy}/g\text{-C}_3\text{N}_4$ composite is simultaneously reduced in $\text{SrAl}_2\text{O}_4:\text{Eu,Dy}$ and increased in $g\text{-C}_3\text{N}_4$.

Figure 6b shows the photoluminescence spectra of the $\text{SrAl}_2\text{O}_4:\text{Eu,Dy-50 wt.}\%$ $g\text{-C}_3\text{N}_4$ with varying an amount of SiO_2 as a binding reagent. Additional SiO_2 -binder results in suppression the 455 nm $g\text{-C}_3\text{N}_4$ peak. Precisely, the $g\text{-C}_3\text{N}_4$ peak decreased to 50% in 0.005M SiO_2 and to 20% in 0.2M SiO_2 samples. The variation in $g\text{-C}_3\text{N}_4$ emission peak with increase in silica exhibits the extent of energy suppression or dissipation in the SiO_2 -layer. The emission light dissipation is observed in non-luminescent YVO_4 coupled with $g\text{-C}_3\text{N}_4$ was also linked to charge transfer [16]. Similarly, where light emission is to be preserved, the lowest SiO_2 -binder is required for sustaining the practical application.

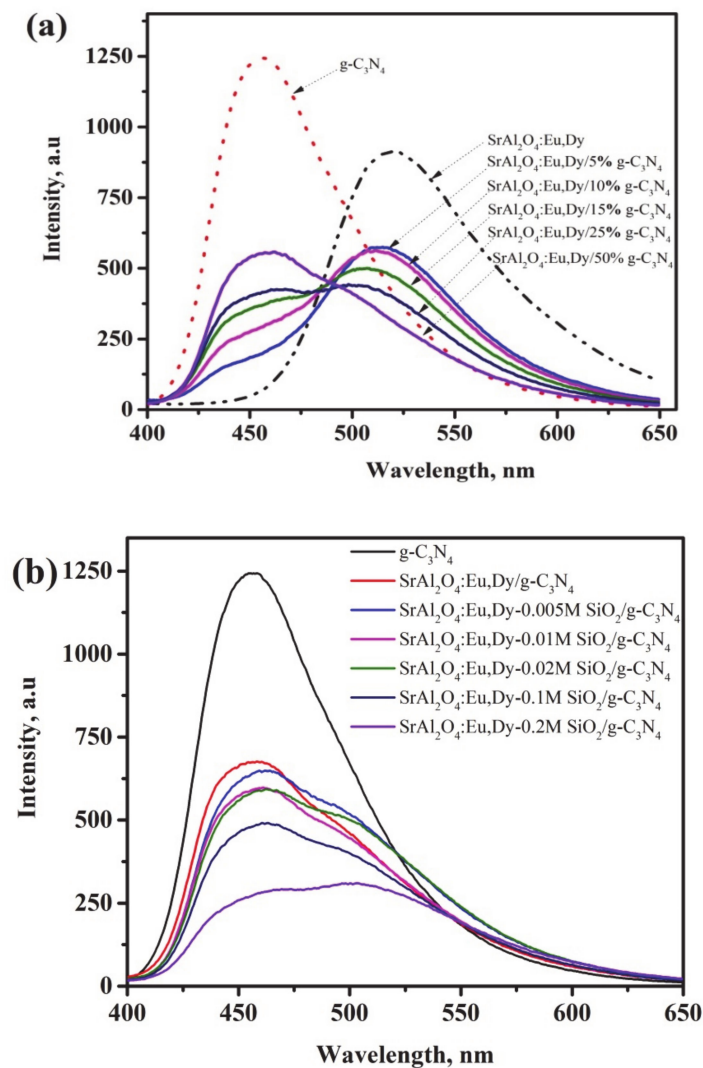


Figure 6. Photoluminescence spectra for (a) the SrAl₂O₄:Eu,Dy/g-C₃N₄ and (b) for SrAl₂O₄:Eu,Dy/50 wt.% g-C₃N₄ with varying SiO₂-binder concentration.

Figure 7 shows the visible light photocatalytic efficiencies for the g-C₃N₄/SrAl₂O₄:Eu,Dy composites. The physically mixed SrAl₂O₄:Eu,Dy and g-C₃N₄ (SrAl₂O₄:Eu,Dy + g-C₃N₄) at 1:1 wt% ratio show an improvement in photocatalytic activity as compared to only g-C₃N₄ sample. However, the 60-min cycle is exhibiting completion of reaction in the thermally treated SrAl₂O₄:Eu,Dy/10 wt.% g-C₃N₄, SrAl₂O₄:Eu,Dy/15 wt.%, SrAl₂O₄:Eu,Dy/25 wt.% g-C₃N₄ and the SrAl₂O₄:Eu,Dy/50 wt.% g-C₃N₄ with higher efficiencies than the physically mixed SrAl₂O₄:Eu,Dy and g-C₃N₄. Clearly, the coupling of nano crystalline g-C₃N₄ with SrAl₂O₄:Eu,Dy phosphor with thermal treatment improves photocatalytic efficiency. This aspect of photocatalysis improvement in heterogeneous composites emanates from the high electron-hole separation efficiency. Interestingly in the first 15 min, the SrAl₂O₄:Eu,Dy/50 wt.% g-C₃N₄ degraded almost 60% of the MB solutions. Therefore, further work on the effect of SiO₂-binder on photocatalytic activity was investigated on this composite under UV and visible light illumination.

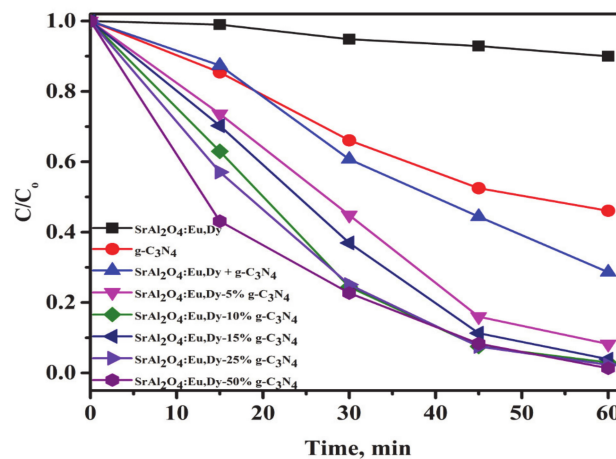


Figure 7. The photodegradation efficiency of MB solution for SrAl₂O₄:Eu,Dy/g-C₃N₄ hybrid composites under visible light solar illumination. Where (SrAl₂O₄:Eu,Dy + g-C₃N₄) is physically mixed at 1:1 wt.% ratio).

Figure 8 shows the photodegradation efficiencies (a) and rate of reaction (b) for the g-C₃N₄ supported on SrAl₂O₄:Eu,Dy/SiO₂ composites in a MB solution under UV-light irradiation. At a glance, pure nano crystalline g-C₃N₄ degrades only 40% of MB solution while photocatalytic efficiencies for the composites of g-C₃N₄-supported SrAl₂O₄:Eu,Dy with and without SiO₂ are enhanced to 90% in a 240-min cycle. The photocatalytic degradation efficiency was significantly improved with additional silica-binder of concentration of as low as 0.01M. In contrast, an amount higher than 0.01M SiO₂ binder impedes the photocatalytic activity. In other words, excess silica layer possibly acts as a slight barrier for photocatalysis progression in SrAl₂O₄:Eu,Dy/g-C₃N₄ composites. The UV-photocatalytic reaction proceeds as the 1st order, where in Figure 8b the 0.01M SiO₂ phosphor/g-C₃N₄ composite has the fastest reaction. Table 4 shows the rate constants for the UV photocatalytic reaction. The experimental errors data were inserted in the Supplementary File (Table S1). The silica content of 0.02M, 0.1M and 0.2M shows lower rate constants than the only SrAl₂O₄:Eu,Dy/g-C₃N₄ without SiO₂ binder. Hence, a low silica addition of 0.005–0.01M is the optimum concentration to promote photocatalytic performance. Regardless of the lower specific surface area or pore volume as shown in Table 3, the SrAl₂O₄:Eu,Dy/g-C₃N₄ composite with/without silica binder merely exhibited higher photoactivity than only nano crystalline g-C₃N₄. Therefore, photocatalytic activity in the composites is dependent on the chemical crystallinity and UV-Vis absorption properties.

Table 4. Rate constants for UV-light photoactivity.

Photocatalyst	Rate Constant, min ⁻¹
SrAl ₂ O ₄ :Eu,Dy	7.0 × 10 ⁻⁴
g-C ₃ N ₄	2.7 × 10 ⁻³
SrAl ₂ O ₄ :Eu,Dy/g-C ₃ N ₄	1.1 × 10 ⁻²
SrAl ₂ O ₄ :Eu,Dy/0.005M SiO ₂ -g-C ₃ N ₄	1.2 × 10 ⁻²
SrAl ₂ O ₄ :Eu,Dy/0.01M SiO ₂ -g-C ₃ N ₄	2.0 × 10 ⁻²
SrAl ₂ O ₄ :Eu,Dy/0.02M SiO ₂ -g-C ₃ N ₄	1.0 × 10 ⁻²
SrAl ₂ O ₄ :Eu,Dy/0.1M SiO ₂ -g-C ₃ N ₄	1.1 × 10 ⁻²
SrAl ₂ O ₄ :Eu,Dy/0.2M SiO ₂ -g-C ₃ N ₄	1.1 × 10 ⁻²

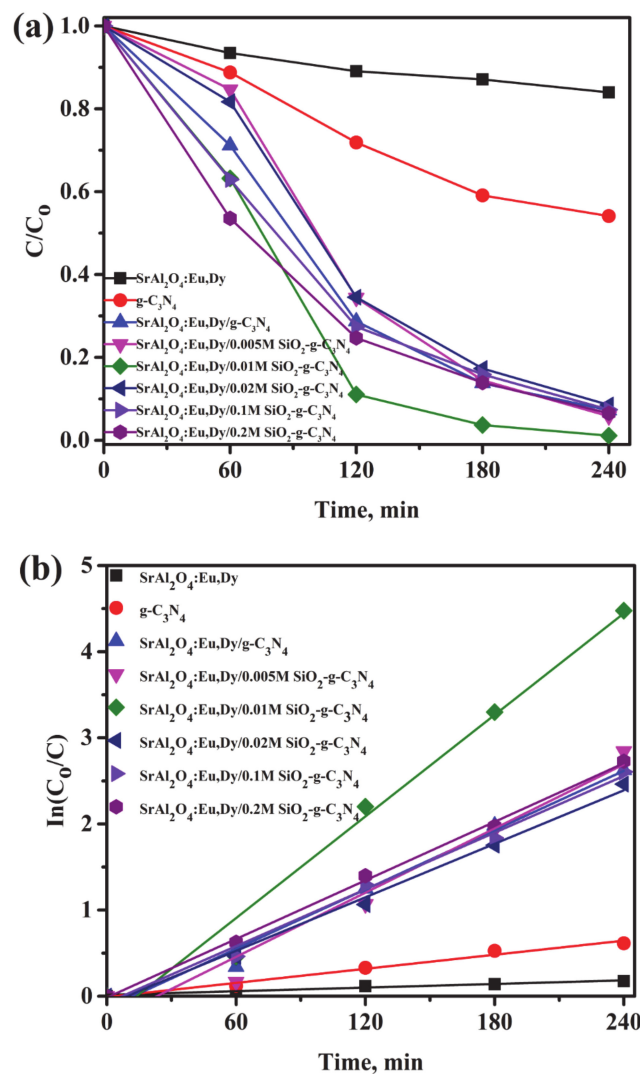


Figure 8. Photo-degradation efficiency (a) and rate of reaction (b) for 50 wt.% $g-C_3N_4$ supported on $SrAl_2O_4:Eu,Dy/SiO_2$ in MB solutions under UV-light illumination.

Figure 9 shows the photo-degradation efficiency (a) and rate of reaction (b) for 50 wt.% $g-C_3N_4$ supported on $SrAl_2O_4:Eu,Dy/SiO_2$ in an MB solution under visible light illumination. The photodegradation reaction proceeded to completion within a 60-min cycle under visible light irradiation. The performance of the $g-C_3N_4$ -phosphor- SiO_2 dominates the nano crystalline $g-C_3N_4$ sample. This is due to the overall improvement in electron-hole separation efficiencies in hybrid composites. The extent of visible light performance reaching to above 90% in a 60-min cycle implies that the hybrid composite is a promising candidate for environmental pollutants. The rates of reaction constant shown in Table 5 show that photocatalytic response kinetics are improved with supporting $g-C_3N_4$ on $SrAl_2O_4:Eu,Dy$ phosphor together with additional SiO_2 binder. The experimental errors data were inserted in the Supplementary File (Table S2).

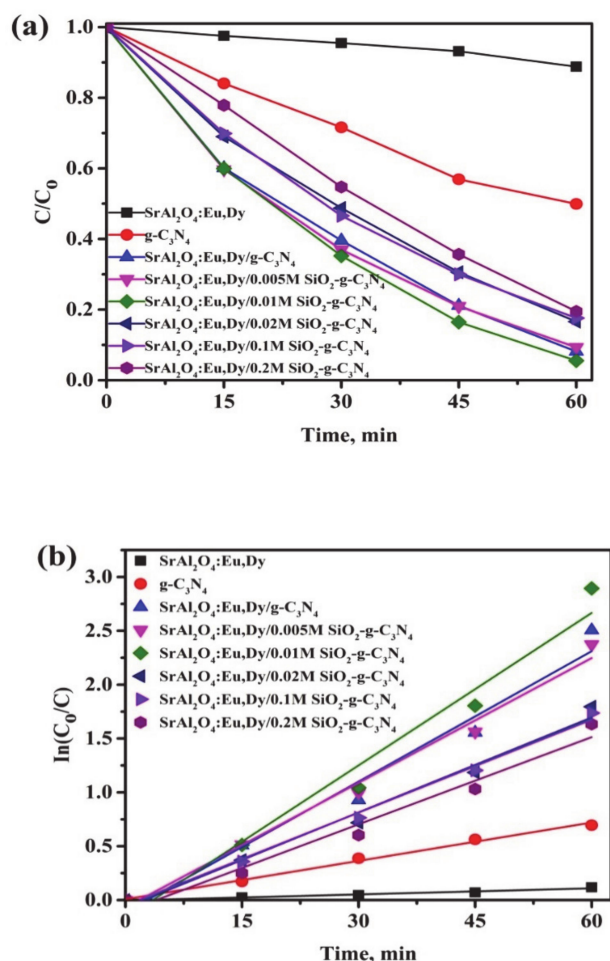


Figure 9. Photo-degradation efficiency (a) and rate of reaction (b) for 50 wt.% $g-C_3N_4$ supported on $SrAl_2O_4:Eu,Dy/SiO_2$ in MB solutions under visible light illuminations.

Table 5. Rate constants for visible light photoactivity.

Photocatalyst	Rate Constant, min^{-1}
$SrAl_2O_4:Eu,Dy$	1.9×10^{-3}
$g-C_3N_4$	1.2×10^{-2}
$SrAl_2O_4:Eu,Dy/g-C_3N_4$	4.0×10^{-2}
$SrAl_2O_4:Eu,Dy/0.005M SiO_2-g-C_3N_4$	3.9×10^{-2}
$SrAl_2O_4:Eu,Dy/0.01M SiO_2-g-C_3N_4$	4.7×10^{-2}
$SrAl_2O_4:Eu,Dy/0.02M SiO_2-g-C_3N_4$	2.9×10^{-2}
$SrAl_2O_4:Eu,Dy/0.1M SiO_2-g-C_3N_4$	2.9×10^{-2}
$SrAl_2O_4:Eu,Dy/0.2M SiO_2-g-C_3N_4$	2.7×10^{-2}

Figure 10 shows MB degradation efficiency by reusing 50% $g-C_3N_4$ -supported on $SrAl_2O_4:Eu,Dy-0.01M SiO_2$ composite. The photocatalytic recyclability test was performed in 4 cycles (240-min per cycle) and showed that the $g-C_3N_4$ -coated $SrAl_2O_4:Eu,Dy/SiO_2$ composite has exceptional photostability with a degradation efficiency above 90% in successive cycles. The $g-C_3N_4$ -coated $SrAl_2O_4:Eu,Dy/SiO_2$ composite exhibits stability in the four cycles which is an important property for catalysts.

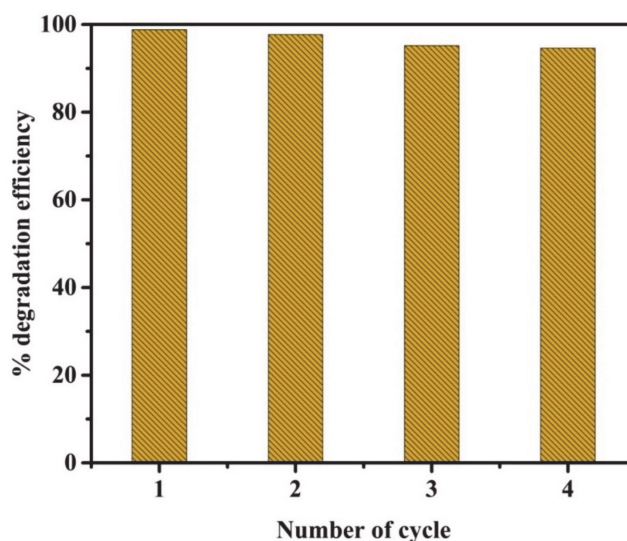


Figure 10. Photocatalytic recyclability test of 50 wt.% $g\text{-C}_3\text{N}_4$ supported on $\text{SrAl}_2\text{O}_4:\text{Eu,Dy}-0.01\text{M SiO}_2$.

Figure 11 shows a schematic diagram for the photocatalysis mechanism in the MB- $\text{SrAl}_2\text{O}_4:\text{Eu,Dy}-\text{SiO}_2/g\text{-C}_3\text{N}_4$ photoreaction mixture. Methylene blue has negligible effects on photocatalytic activity [47]. On the same note, $\text{SrAl}_2\text{O}_4:\text{Eu,Dy}$ phosphor is reported to exhibit negligible photocatalytic activity in aqueous RhB dye solutions. Moreover, its unique energy levels absorb even visible light and emit a blue fluorescence which sustains a photocatalytic reaction [40]. Silica was added at a molar ratio to perform a binding role between phosphor and $g\text{-C}_3\text{N}_4$. Since heterojunction interfaces exist in composite materials [48], even visible light would be sensitized by the $\text{SrAl}_2\text{O}_4:\text{Eu,Dy}/g\text{-C}_3\text{N}_4$. As observed in Figure 7, the thermally treated $\text{SrAl}_2\text{O}_4:\text{Eu,Dy}/g\text{-C}_3\text{N}_4$ composites exhibited higher efficiencies than physically mixed $\text{SrAl}_2\text{O}_4:\text{Eu,Dy}$ and $g\text{-C}_3\text{N}_4$. Therefore, thermal treatment is beneficial in the formation of heterojunctions.

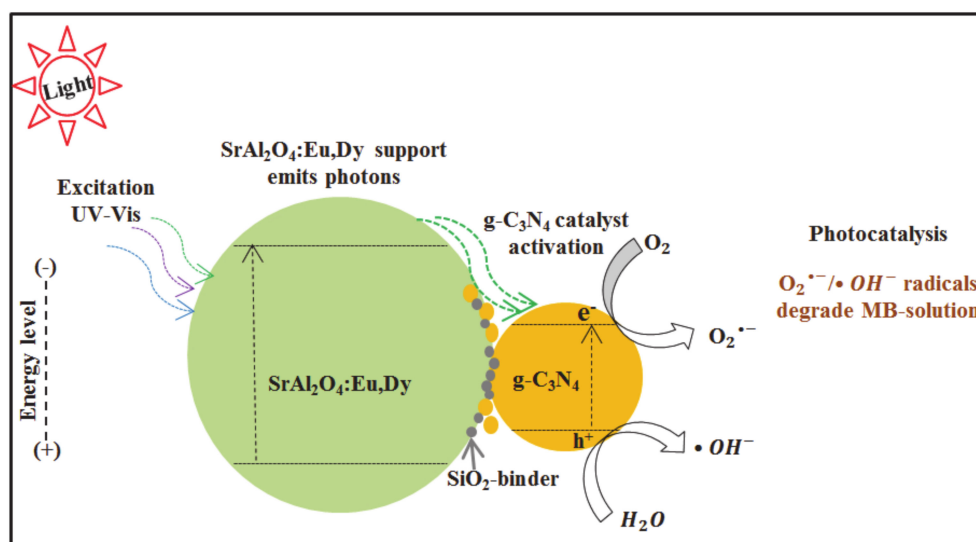


Figure 11. Schematic diagram for photocatalysis mechanism for the MB- $\text{SrAl}_2\text{O}_4:\text{Eu,Dy}-\text{SiO}_2/g\text{-C}_3\text{N}_4$ photoreaction mixture.

$\text{SrAl}_2\text{O}_4:\text{Eu,Dy}$ phosphor performs the role of sensitizing UV or partial visible light photons and releasing visible light photons. Then, the $g\text{-C}_3\text{N}_4$ catalyst is activated by photons $\lambda < 460\text{ nm}$ or even visible light photons from phosphor through the $\text{SrAl}_2\text{O}_4:\text{Eu,Dy}/g\text{-C}_3\text{N}_4$ heterojunction. Then, the activated $g\text{-C}_3\text{N}_4$ releases electrons which are adsorbed to oxygen whilst holes are

adsorbed to water molecules forming superoxide and hydroxide radicals which attack and decompose the MB-dye structure.

Photocatalytic reactions of SrAl₂O₄:Eu,Dy phosphor-g-C₃N₄ composite supported with thin silica-binding (0.01M SiO₂) layer proceeds faster than the only g-C₃N₄. With SiO₂ in large amounts of 0.02M, 0.1M, and 0.2M, the photocatalytic activity was reduced, which means that the interfacial (contact) junction between SrAl₂O₄:Eu,Dy and g-C₃N₄ was disrupted. Thus, the SrAl₂O₄:Eu,Dy support forms a heterojunction with the g-C₃N₄ catalyst (with or without SiO₂-binder layer).

4. Discussion

The phosphor SrAl₂O₄:Eu,Dy support synthesized by solution combustion and sintering at 1100 °C for 1 h exhibited broad photoluminescence at 525 nm. In this research, sintering at 1100 °C for 1 h produce stable support at lower energy consumption than the solid-state sintering at 1300–1500 °C for 2–6 h dwelling time [30]. Particle agglomeration is unavoidable since sintering promotes grain growth. Therefore, to improve particle dispersion on agglomerated SrAl₂O₄:Eu,Dy phosphor a pulverizing or mixing step is necessary.

SrAl₂O₄:Eu,Dy support and g-C₃N₄ catalyst have strong absorption in the UV-region. Interestingly, by coupling these two materials unique optical properties were observed through shift of UV-Vis diffuse reflectance absorption spectra towards the visible light region in Figure 5. Additional SiO₂ between SrAl₂O₄:Eu,Dy phosphor and g-C₃N₄ also weakened the g-C₃N₄ peak. Thus, Silica act as energy dissipation centres. This phenomenon of energy dissipation was also observed in Al₂O₃ coupled with CaAl₂O₄:Eu,Nd/TiO₂ long lasting phosphor [49].

According to one research, when g-C₃N₄ and SiO₂ were coupled, higher (50 wt.%) silica resulted in the lowest PL emission intensities but with most superior catalytic property [15]. Moreover, these composites were reported to fortunately possess exceptionally large surface areas of more than 100 m²/g. These results contradict with our result in Figure 6, where g-C₃N₄/SiO₂ supported on light emitting phosphor suppressed both the PL intensities and photocatalytic properties. Therefore, it is possible to tune the photocatalytic property by combining with long-lasting phosphor to observe enhanced activity at low silica addition.

In our work, we focused on the photocatalytic effects of SrAl₂O₄:Eu,Dy-0.01M SiO₂/50 wt.% g-C₃N₄ which exhibited a red-shift in the diffuse reflectance absorption. Therefore, we recommend further investigations in the evaluation of quantum efficiencies in relation to photocatalytic efficiencies.

5. Conclusions

Graphitic carbon nitride (g-C₃N₄) was supported on SrAl₂O₄:Eu,Dy with or without a SiO₂-binding agent. The g-C₃N₄-SrAl₂O₄:Eu,Dy composites exhibit unique broadened photoluminescence emission spectra with their respective dominant emission peaks at 450 nm and 525 nm. Silica additions as a binder between g-C₃N₄ and SrAl₂O₄:Eu,Dy act as energy dissipation centers for light emitted from phosphor. The UV-Vis light photocatalytic performances are improved several times in the composite of g-C₃N₄-supported SrAl₂O₄:Eu,Dy as compared to pure g-C₃N₄. The photocatalytic efficiency was improved with an addition of low SiO₂ amount as a binding reagent. However, a higher SiO₂-coating layer acts as a barrier to the photodegradation efficiencies. Thermally treating SrAl₂O₄:Eu,Dy-g-C₃N₄ composites is beneficial for the improved photodegradation of methylene blue pollutants.

Supplementary Materials: The following are available online at <http://www.mdpi.com/2079-6412/10/10/917/s1>, Figure S1: Spectra for UV-light, Figure S2: The Xe lamp spectra (Solsim 395), Table S1: Rate constants for UV-light photoactivity, Table S2: Rate constants for visible light photoactivity.

Author Contributions: Supervision, J.-S.K.; writing—original draft preparation, S.M. All authors have read and agreed to the published version of the manuscript.

Funding: This study was supported by a grant (20CTAP-C157721-01) from Infrastructure and transportation technology promotion research program funded by Ministry of Land, Infrastructure and Transport of Korean government.

Conflicts of Interest: The authors declare no conflict of interest.

References

1. Gupta, S.M.; Tripathi, M. A review of TiO₂ nanoparticles. *Chin. Sci. Bull.* **2011**, *56*, 1639–1657. [[CrossRef](#)]
2. Fujishima, A.; Rao, T.N.; Tryk, D.A. Titanium dioxide photocatalysis. *J. Photochem. Photobiol. C Photochem. Rev.* **2000**, *1*, 1–21. [[CrossRef](#)]
3. Wu, P.; Wang, J.; Zhao, J.; Guo, L.; Osterloh, F.E. Structure defects in g-C₃N₄ limit visible light driven hydrogen evolution and photovoltage. *J. Mater. Chem. A* **2014**, *2*, 20338–20344. [[CrossRef](#)]
4. He, Y.; Wang, Y.; Zhang, L.; Teng, B.; Fan, M. High-efficiency conversion of CO₂ to fuel over ZnO/g-C₃N₄ photocatalyst. *Appl. Catal. B Environ.* **2015**, *168*, 1–8. [[CrossRef](#)]
5. Li, W.; Wang, L.; Zhang, Q.; Chen, Z.; Deng, X.; Feng, C.; Xu, L.; Sun, M. Fabrication of an ultrathin 2D/2D C₃N₄/MoS₂ heterojunction photocatalyst with enhanced photocatalytic performance. *J. Alloys Compd.* **2019**, *808*, 151681. [[CrossRef](#)]
6. Ruan, D.; Kim, S.; Fujitsuka, M.; Majima, T. Defects rich g-C₃N₄ with mesoporous structure for efficient photocatalytic H₂ production under visible light irradiation. *Appl. Catal. B Environ.* **2018**, *238*, 638–646. [[CrossRef](#)]
7. Jin, Z.; Zhang, Q.; Yuan, S.; Ohno, T. Synthesis high specific surface area nanotube g-C₃N₄ with two-step condensation treatment of melamine to enhance photocatalysis properties. *RSC Adv.* **2015**, *5*, 4026–4029. [[CrossRef](#)]
8. Wang, X.L.; Yang, H.G. Facile fabrication of high-yield graphitic carbon nitride with a large surface area using bifunctional urea for enhanced photocatalytic performance. *Appl. Catal. B Environ.* **2017**, *205*, 624–630. [[CrossRef](#)]
9. Chen, Q.; Hou, H.; Zhang, D.; Hu, S.; Min, T.; Liu, B.; Yang, C.; Pu, W.; Hu, J.; Yang, J. Enhanced visible-light driven photocatalytic activity of hybrid ZnO/g-C₃N₄ by high performance ball milling. *J. Photochem. Photobiol. A Chem.* **2018**, *350*, 1–9. [[CrossRef](#)]
10. Xu, J.; Zhang, L.; Shi, R.; Zhu, Y. Chemical exfoliation of graphitic carbon nitride for efficient heterogeneous photocatalysis. *J. Mater. Chem. A* **2013**, *1*, 14766–14772. [[CrossRef](#)]
11. Liao, G.; Gong, Y.; Zhang, L.; Gao, H.; Yang, G.-J.; Fang, B. Semiconductor polymeric graphitic carbon nitride photocatalysts: The “holy grail” for the photocatalytic hydrogen evolution reaction under visible light. *Energy Environ. Sci.* **2019**, *12*, 2080–2147. [[CrossRef](#)]
12. Li, Y.; Sun, Y.; Ho, W.; Zhang, L.L.; Huang, H.; Cai, Q.; Dong, F. Highly enhanced visible-light photocatalytic NO_x purification and conversion pathway on self-structurally modified g-C₃N₄ nanosheets. *Sci. Bull.* **2018**, *63*, 609–620. [[CrossRef](#)]
13. Wang, S.; Hua, X.; Ji, J.; Cai, Z.; Zhao, Y. Facile synthesis of highly efficient mpg-C₃N₄/TiO₂ visible-light-induced photocatalyst and its formaldehyde removal performance in coating application. *J. Nanopart. Res.* **2019**, *21*, 187. [[CrossRef](#)]
14. Zhou, S.; Liu, Y.; Li, J.; Wang, Y.; Jiang, G.; Zhao, Z.; Wang, D.; Duan, A.; Liu, J.; Wei, Y. Facile in situ synthesis of graphitic carbon nitride (g-C₃N₄)-N-TiO₂ heterojunction as an efficient photocatalyst for the selective photoreduction of CO₂ to CO. *Appl. Catal. B Environ.* **2014**, *158*, 20–29. [[CrossRef](#)]
15. Peng, L.; Li, Z.-W.; Zheng, R.-R.; Yu, H.; Dong, X.-T. Preparation and characterization of mesoporous g-C₃N₄/SiO₂ material with enhanced photocatalytic activity. *J. Mater. Res.* **2019**, *34*, 1785–1794. [[CrossRef](#)]
16. Cai, J.; He, Y.; Wang, X.; Zhang, L.; Dong, L.; Lin, H.; Zhao, L.; Yi, X.; Weng, W.; Wan, H. Photodegradation of RhB over YVO₄/g-C₃N₄ composites under visible light irradiation. *RSC Adv.* **2013**, *3*, 20862. [[CrossRef](#)]
17. Peng, L.; Zheng, R.-R.; Feng, D.-W.; Yu, H.; Dong, X. Synthesis of eco-friendly porous g-C₃N₄/SiO₂/SnO₂ composite with excellent visible-light responsive photocatalysis. *Arab. J. Chem.* **2020**, *13*, 4275–4285. [[CrossRef](#)]
18. Vattikuti, S.P.; Byon, C. Hydrothermally synthesized ternary heterostructured MoS₂/Al₂O₃/g-C₃N₄ photocatalyst. *Mater. Res. Bull.* **2017**, *96*, 233–245. [[CrossRef](#)]
19. Di, L.; Yang, H.; Xian, T.; Chen, X. Construction of Z-Scheme g-C₃N₄/CNT/Bi₂Fe₄O₉ Composites with Improved Simulated-Sunlight Photocatalytic Activity for the Dye Degradation. *Micromachines* **2018**, *9*, 613. [[CrossRef](#)]

20. Zhang, C.; Li, Y.; Shuai, D.; Shen, Y.; Xiong, W.; Wang, L. Graphitic carbon nitride (g-C₃N₄)-based photocatalysts for water disinfection and microbial control: A review. *Chemosphere* **2019**, *214*, 462–479. [[CrossRef](#)]
21. Zhang, W.; Zhou, L.; Shi, J.; Deng, H. Synthesis of Ag₃PO₄/G-C₃N₄ Composite with Enhanced Photocatalytic Performance for the Photodegradation of Diclofenac under Visible Light Irradiation. *Catalysts* **2018**, *8*, 45. [[CrossRef](#)]
22. Zhao, Z.; Zhang, X.; Fan, J.; Xue, D.; Zhang, B.; Yin, S. N-TiO₂/g-C₃N₄/Up-conversion phosphor composites for the full-spectrum light-responsive deNO_x photocatalysis. *J. Mater. Sci.* **2018**, *53*, 7266–7278. [[CrossRef](#)]
23. Ye, S.; Wang, R.; Wu, M.; Yuan, Y. A review on g-C₃N₄ for photocatalytic water splitting and CO₂ reduction. *Appl. Surf. Sci.* **2015**, *358*, 15–27. [[CrossRef](#)]
24. Mamba, G.; Mishra, A.K. Graphitic carbon nitride (g-C₃N₄) nanocomposites: A new and exciting generation of visible light driven photocatalysts for environmental pollution remediation. *Appl. Catal. B Environ.* **2016**, *198*, 347–377. [[CrossRef](#)]
25. Huang, Y.; Zhang, X.; Zhang, K.; Lu, P.; Zhang, D. Facile fabrication of sandwich-like BiOI/AgI/g-C₃N₄ composites for efficient photocatalytic degradation of methyl orange and reduction of Cr(VI). *J. Nanopart. Res.* **2018**, *20*, 328. [[CrossRef](#)]
26. Li, H.; Yin, S.; Wang, Y.; Sato, T. Persistent luminescence assisted photocatalytic properties of CaAl₂O₄:(Eu,Nd)/TiO_{2-x}N_y and Sr₄Al₁₄O₂₅:(Eu,Dy)/TiO_{2-x}N_y. *J. Mol. Catal. A: Chem.* **2012**, 129–133. [[CrossRef](#)]
27. Zargoosh, K.; Aliabadi, H.M. SrAl₂O₄:Eu²⁺: Dy³⁺/WO₃/polyester nanocomposite as a highly efficient and environmentally friendly photocatalyst for removal of dyes from industrial wastes. *Environ. Nanotechnol. Monit. Manag.* **2019**, *12*, 100273. [[CrossRef](#)]
28. Demirci, S.; Gültekin, S.; Akalin, S.A.; Oter, O.; Ertekin, K.; Çelik, E. Synthesis and spectral characterization of Sr₄Al₁₄O₂₅:Eu²⁺/Dy³⁺ blue-green phosphorous powders by sol-gel method. *Mater. Sci. Semicond. Process.* **2015**, *31*, 611–617. [[CrossRef](#)]
29. Sung, H.-J.; Kim, B.-M.; Jung, S.-C.; Kim, J.-S. Photocatalytic Characteristics for The Nanocrystalline TiO₂ Supported On Sr₄Al₁₄O₂₅: Eu²⁺, Dy³⁺ Phosphor Beads. *Adv. Mater. Lett.* **2016**, *7*, 36–41. [[CrossRef](#)]
30. Rojas-Hernandez, R.E.; Rubio-Marcos, F.; Rodriguez, M.A.; Fernández, J.F. Long lasting phosphors: SrAl₂O₄:Eu, Dy as the most studied material. *Renew. Sustain. Energy Rev.* **2018**, *81*, 2759–2770. [[CrossRef](#)]
31. Rojas-Hernandez, R.E.; Rodríguez, M.A.; Rubio-Marcos, F.; Serrano, A.; Fernández, J.F. Designing nanostructured strontium aluminate particles with high luminescence properties. *J. Mater. Chem. C* **2015**, *3*, 1268–1276. [[CrossRef](#)]
32. Havasi, V.; Vödrédi, B.; Kukovecz, Á. Photocatalytic performance of Sr₄Al₁₄O₂₅: Eu,Dy phosphor assisted ZnO:Co⁺ Ag nanocomposite under continuous and pulsed illumination. *Catal. Today* **2017**, *284*, 107–113. [[CrossRef](#)]
33. Yuan, Y.; Cao, S.-W.; Liao, Y.; Yin, L.-S.; Xue, C. Red phosphor/g-C₃N₄ heterojunction with enhanced photocatalytic activities for solar fuels production. *Appl. Catal. B Environ.* **2013**, *140*, 164–168. [[CrossRef](#)]
34. Lam, S.-M.; Sin, J.-C.; Mohamed, A.R. A review on photocatalytic application of g-C₃N₄/semiconductor (CNS) nanocomposites towards the erasure of dyeing wastewater. *Mater. Sci. Semicond. Process.* **2016**, *47*, 62–84. [[CrossRef](#)]
35. Sun, Z.; Wang, H.; Wu, Z.; Wang, L. g-C₃N₄ based composite photocatalysts for photocatalytic CO₂ reduction. *Catal. Today* **2018**, *300*, 160–172. [[CrossRef](#)]
36. Foye, C. The Relationship Between Size of Living Space and Subjective Well-Being. *J. Happiness Stud.* **2016**, *18*, 427–461. [[CrossRef](#)]
37. Saiful Amran, S.N.B.; Wongso, V.; Abdul Halim, N.S.; Husni, M.K.; Sambudi, N.S.; Wirzal, M.D.H. Immobilized carbon-doped TiO₂ in polyamide fibers for the degradation of methylene blue. *J. Asian Ceram. Soc.* **2019**, *7*, 321–330. [[CrossRef](#)]
38. Sun, H.; Pan, L.; Piao, X.; Sun, Z. Long afterglow SrAl₂O₄: Eu,Dy phosphors for CdS quantum dot-sensitized solar cells with enhanced photovoltaic performance. *J. Mater. Chem. A* **2013**, *1*, 6388. [[CrossRef](#)]
39. Yin, H.; Chen, X.; Hou, R.; Zhu, H.; Li, S.; Huo, Y.; Li, H. Ag/BiOBr Film in a Rotating-Disk Reactor Containing Long-Afterglow Phosphor for Round-the-Clock Photocatalysis. *ACS Appl. Mater. Interfaces* **2015**, *7*, 20076–20082. [[CrossRef](#)]

40. Liu, X.; Chen, X.; Li, Y.; Wu, B.; Luo, X.; Ouyang, S.; Luo, S.; Al Kheraif, A.A.; Lin, J. A g-C₃N₄@Au@SrAl₂O₄:Eu²⁺, Dy³⁺ composite as an efficient plasmonic photocatalyst for round-the-clock environmental purification and hydrogen evolution. *J. Mater. Chem. A* **2019**, *7*, 19173–19186. [[CrossRef](#)]
41. Sikandar, M.A.; Ahmad, W.; Khan, M.H.; Ali, F.; Waseem, M. Effect of water resistant SiO₂ coated SrAl₂O₄:Eu²⁺ Dy³⁺ persistent luminescence phosphor on the properties of Portland cement pastes. *Constr. Build. Mater.* **2019**, *228*, 116823. [[CrossRef](#)]
42. Li, X.; Li, Y.; Sun, G.; Luo, N.; Zhang, B.; Zhang, Z. Synthesis of a Flower-Like g-C₃N₄/ZnO Hierarchical Structure with Improved CH₄ Sensing Properties. *Nanomaterials* **2019**, *9*, 724. [[CrossRef](#)] [[PubMed](#)]
43. Wang, X.; Wang, S.; Hu, W.; Cai, J.; Zhang, L.; Dong, L.; Zhao, L.; He, Y. Synthesis and photocatalytic activity of SiO₂/g-C₃N₄ composite photocatalyst. *Mater. Lett.* **2014**, *115*, 53–56. [[CrossRef](#)]
44. Sudhaik, A.; Raizada, P.; Shandilya, P.; Jeong, D.-Y.; Lim, J.-H.; Singh, P. Review on fabrication of graphitic carbon nitride based efficient nanocomposites for photodegradation of aqueous phase organic pollutants. *J. Ind. Eng. Chem.* **2018**, *67*, 28–51. [[CrossRef](#)]
45. Mavengere, S.; Jung, S.-C.; Kim, J.-S. Visible Light Photocatalytic Activity of NaYF₄:(Yb,Er)-CuO/TiO₂ Composite. *Catalysts* **2018**, *8*, 521. [[CrossRef](#)]
46. Kim, J.-S.; Kim, S.-W.; Jung, S.-C. Photocatalytic reaction characteristics of the titanium dioxide supported on the long phosphorescent phosphor by a low pressure chemical vapor deposition. *J. Nanosci. Nanotechnol.* **2014**, *14*, 7751–7755. [[CrossRef](#)] [[PubMed](#)]
47. Mavengere, S.; Kim, J.-S. UV–visible light photocatalytic properties of NaYF₄:(Gd, Si)/TiO₂ composites. *Appl. Surf. Sci.* **2018**, *444*, 491–496. [[CrossRef](#)]
48. Hu, M.; Xing, Z.; Cao, Y.; Li, Z.; Yan, X.; Xiu, Z.; Zhao, T.; Yang, S.; Zhou, W. Ti³⁺ self-doped mesoporous black TiO₂/SiO₂/g-C₃N₄ sheets heterojunctions as remarkable visible-lightdriven photocatalysts. *Appl. Catal. B Environ.* **2018**, *226*, 499–508. [[CrossRef](#)]
49. Yoon, J.-H.; Jung, S.-C.; Kim, J.-S. Photocatalytic effects for the TiO₂-coated phosphor materials. *Mater. Chem. Phys.* **2011**, *125*, 342–346. [[CrossRef](#)]



© 2020 by the authors. Licensee MDPI, Basel, Switzerland. This article is an open access article distributed under the terms and conditions of the Creative Commons Attribution (CC BY) license (<http://creativecommons.org/licenses/by/4.0/>).